PHYSICS OF PLASMAS **14**, 013508 (2007)

Effects of non-Maxwellian electron velocity distribution function on two-stream instability in low-pressure discharges

D. Sydorenko[a] and A. Smolyakov
Department of Physics and Engineering Physics, University of Saskatchewan, Saskatoon, Saskatchewan S7N 5E2, Canada

I. Kaganovich and Y. Raitses
Princeton Plasma Physics Laboratory, Princeton University, Princeton, New Jersey 08543

(Received 26 September 2006; accepted 28 December 2006; published online 31 January 2007)

Electron emission from discharge chamber walls is important for plasma maintenance in many low-pressure discharges. The electrons emitted from the walls are accelerated by the sheath electric field and are injected into the plasma as an electron beam. Penetration of this beam through the plasma is subject to the two-stream instability, which tends to slow down the beam electrons and heat the plasma electrons. In the present paper, a one-dimensional particle-in-cell code is used to simulate these effects both in a collisionless plasma slab with immobile ions and in a cross-field discharge of a Hall thruster. The two-stream instability occurs if the total electron velocity distribution function of the plasma-beam system is a nonmonotonic function of electron speed. Low-pressure plasmas can be depleted of electrons with energy above the plasma potential. This study reveals that under such conditions the two-stream instability depends crucially on the velocity distribution function of electron emission. It is shown that propagation of the secondary electron beams in Hall thrusters may be free of the two-stream instability if the velocity distribution of secondary electron emission is a monotonically decaying function of speed. In this case, the beams propagate between the walls with minimal loss of the beam current and the secondary electron emission does not affect the thruster plasma properties.
[DOI: 10.1063/1.2435315]

I. INTRODUCTION

In many discharges (e.g., capacitively coupled plasmas, divertor plasmas, multipactors, dc hollow cathode discharges, dc magnetrons, electrostatic and Hall thrusters) there are electron-emitting surfaces: walls with secondary electron emission (SEE), thermionic cathodes, photocathodes, etc.[1] Electrons emitted from such a surface are accelerated into the plasma by the intense electric field in the sheath adjacent to the surface and form an electron beam. These beams of emitted electrons play an important part in the discharge maintenance and affect plasma and sheath characteristics.[2,3]

In low-pressure discharges, in which the electron collisions with other particles are infrequent, the two-stream instability[4,5] can be the major factor affecting propagation of emitted electrons through the plasma. The interaction of beam electrons with resonant waves during the two-stream instability slows down some electrons and accelerates others, dispersing the beam electron velocity distribution function (EVDF). Some plasma electrons may also interact with the excited waves, modifying the plasma EVDF. This modification eventually affects the particle and energy fluxes in the plasma, especially at the wall. This effect is relevant, e.g., to the temperature saturation in Hall thrusters,[6] or to the thermal instability due to the plasma-wall coupling in tokamaks.[7] During the two-stream instability, the amplitude of the wave (or waves) resonant with the beam grows exponentially until it reaches some saturation level.[8–11] The instability develops if the number of beam electrons transferring energy to the resonant wave exceeds the number of electrons absorbing energy from the wave. This corresponds to the condition that the one-dimensional EVDF of the beam-plasma system $f(v)$ must be an increasing function of speed in some velocity interval, violating the following formal criterion of stability:[12]

$$\frac{\partial}{\partial(v^2)} f(v) \leqslant 0 \quad \text{for} \quad -\infty < v < \infty, \tag{1}$$

where v is the velocity parallel to the direction of beam propagation. Note that form (1) of the stability criterion is independent on the direction of beam propagation ($v>0$ or $v<0$).

Theories and numerical simulations of the two-stream instability usually consider a beam on the tail of a Maxwellian plasma EVDF. Frequently, periodic boundary conditions are assumed for plasma-beam systems.[8–11,13] This assumption substantially simplifies the calculations. In such a system, perturbations are periodic in space and grow with time. In a nonperiodic plasma system with an electron-emitting boundary, the beam EVDF at the point of its origin is intact, unaffected by the instability. The beam EVDF starts as the velocity distribution function of electron emission (VDFEE) defined solely by the properties of the emission mechanism. The intensity of the two-stream instability grows as the beam traverses the system.[14]

[a]Present address: Department of Physics, University of Alberta, Edmonton, Alberta T6G 2G7, Canada. Electronic address: sydorenk@ualberta.ca

To correctly describe the two-stream instability and, hence, the penetration of emitted electrons into the plasma, an accurate kinetic description is necessary for both plasma and emitted electrons. To this end, for modeling of realistic discharges it is important to take into account that the plasma EVDF is depleted of electrons with energy above the plasma potential. The present paper uses particle-in-cell (PIC) simulations to show that the development of the two-stream instability in a low-pressure discharge with electron-emitting walls depends crucially on the VDFEE. For different types of VDFEE, the two-stream instability either is observed for the entire duration of electron emission, or vanishes soon after the emission starts, or does not occur at all. The instability does not occur if the emission is too weak to make the total EVDF a nonmonotonic function of electron velocity in the direction of beam propagation. *Note that this is possible due to the depletion of the plasma EVDF for energies above the plasma potential in low-pressure discharges (in contrast to the case of a Maxwellian plasma EVDF, in which the emitted beams always cause an instability).* The effect of vanishing instability relies largely on the modification of the velocity distribution function of electrons confined by the plasma potential.

The paper is organized as follows. In Sec. II, criterion (1) is applied for qualitative examination of stability of a bounded collisionless plasma-beam system for monotonic and nonmonotonic VDFEE. Section III shows the results of PIC simulations with two different types of the VDFEE, immobile ions, and constant emission. In Sec. IV, the results obtained with simplified approach in Secs. II and III are verified using more realistic Hall thruster model simulations. Concluding remarks are given in Sec. V.

II. QUALITATIVE ANALYSIS OF DIFFERENT TYPES OF VDFEE

It is instructive to start analysis with the EVDF in a one-dimensional collisionless plasma bounded by electron-emitting walls, omitting the perturbations due to the two-stream instability. Provided both walls have the same electrical and emission properties, and the emission is not in the space-charge limited regime,[15] the profile of the electrostatic potential in the plasma $\Phi(x)$ is symmetric, with maximum Φ_p in the plasma center, and monotonically decaying towards the walls, where it is selected to be zero [see Fig. 1(a)]. Assume that the electron mean free path between collisions with other particles λ is larger than or comparable to the distance between the walls L. The plasma EVDF is then depleted of electrons with positive total energy $\varepsilon_x = w_x - e\Phi(x) > 0$, or $w_x > e\Phi(x)$, where $w_x = mv_x^2/2$ is the electron kinetic energy, $e\Phi(x)$ plays the role of the confinement threshold energy, and m, $-e$, and v_x are the electron mass, charge, and velocity, respectively.[16,17] A schematic of such an EVDF is shown in Fig. 1(b). The plasma EVDF may be approximated by a cutoff Maxwellian EVDF:

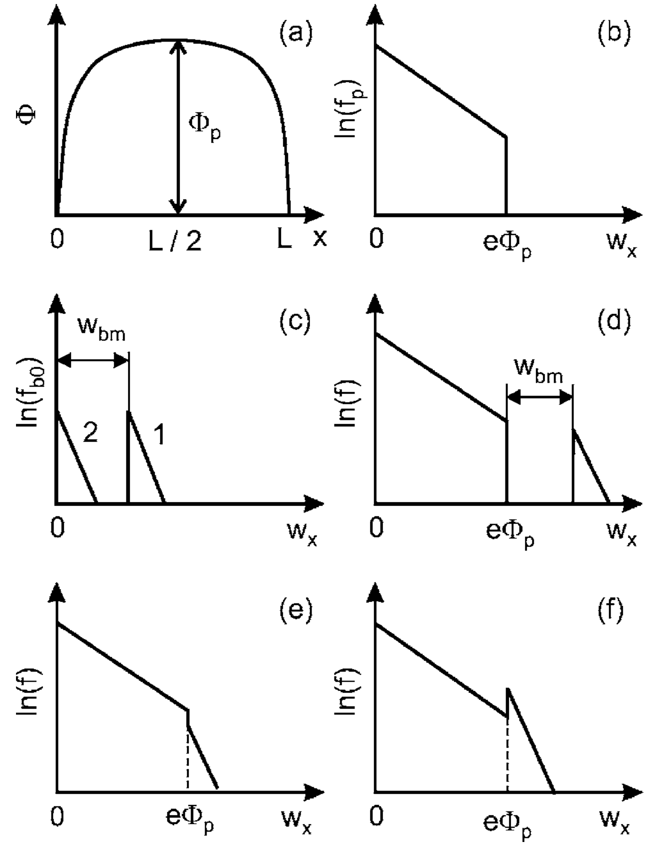

FIG. 1. Schematic diagrams. (a) Profile of the electrostatic potential $\Phi(x)$ in a bounded one-dimensional plasma. (b) EVDF of the plasma in the collisionless regime $\lambda \geqslant L$. (c) Two simplified cases of the VDFEE f_{b0}: a half-Maxwellian EVDF "shifted" along the energy axis by $w_{bm} > 0$ (curve 1), and a half-Maxwellian EVDF with $w_{bm}=0$ (curve 2). (d) The total EVDF of the plasma-beam system with VDFEE given by curve 1 in (c). (e) The total EVDF of the plasma-beam system with VDFEE given by curve 2 in (c) for low density SEE beam, $f_p(v_*, L/2) > f_b(v_*, L/2)$. (f) The total EVDF of the plasma-beam system with VDFEE given by curve 2 in (c) for a high-density beam; i.e., $f_p(v_*, L/2) < f_b(v_*, L/2)$. All EVDFs are plotted as functions of energy w_x for $v_x > 0$; EVDFs in (b), (d), (e), and (f) are plotted at $x = L/2$, and in (c) at $x=0$.

$$f_p(v_x,x) = \begin{cases} \dfrac{n_p}{\pi^{1/2} v_{\mathrm{th},p}\, \mathrm{erf}(v_{*p}/v_{\mathrm{th},p})} \exp\left\{ -\dfrac{v_x^2}{v_{\mathrm{th},p}^2} - \dfrac{e[\Phi_p - \Phi(x)]}{T_p} \right\}, & \text{if} \quad |v_x| < v_*, \\ 0, & \text{if} \quad |v_x| > v_*, \end{cases} \tag{2}$$

where n_p is the plasma electron density at $x=L/2$, $v_{\mathrm{th},p} = (2T_p/m)^{1/2}$ is the thermal velocity of plasma electrons, T_p is the plasma electron temperature (in energy units), $v_* \equiv v_*(x) = [2e\Phi(x)/m]^{1/2}$ is the cutoff velocity, and $v_{*p} \equiv v_*(L/2)$.

For illustrative purposes, we consider the two limiting cases of the VDFEE: a half-Maxwellian EVDF and a half-Maxwellian EVDF "shifted" by some energy w_{bm}. The latter VDFEE, in particular, may represent a sharp peak in the velocity distribution of SEE from a metal surface, which occurs at the energy of the order of the sum of the Fermi energy and the work function of the metal.[18,19] Thus, we assume that the boundary at $x=0$ emits electrons with the following VDFEE:

$$f_{b0}(v_x) = \begin{cases} 0, & \text{if} \quad v_x < v_{bm}, \\ \dfrac{2n_{b0}}{\pi^{1/2} v_{\text{th},b}\,\text{erfc}(v_{bm}/v_{\text{th},b})} \exp\left(-\dfrac{v_x^2}{v_{\text{th},b}^2}\right), & \text{if} \quad v_x \geq v_{bm}, \end{cases} \tag{3}$$

where n_{b0} is the density of emitted electrons near the emitting wall, $v_{\text{th},b}=(2T_b/m)^{1/2}$ is the thermal velocity of emitted electrons, T_b is the effective temperature of emission (in energy units), v_{bm} is the velocity of the VDFEE maximum, $v_{bm} \geq 0$. Note that the density n_{b0} can be expressed via the emission flux Γ as

$$n_{b0} = \frac{\pi^{1/2}\Gamma}{v_{\text{th},b}} \frac{\text{erfc}(v_{bm}/v_{\text{th},b})}{\exp(-v_{bm}^2/v_{\text{th},b}^2)}.$$

The electron emission at $x=L$ is characterized by a VDFEE defined symmetrically to (3) for $v_x < 0$.

In fact, the choice of the VDFEE in form (3) is not unique. For physical processes discussed below, any VDFEE with a single maximum on the interval $0 \leq v_x < \infty$ (for emission at $x=0$) is suitable. It is the position of this velocity maximum which is important: the VDFEE is a nonmonotonic function of speed if $v_{bm} > 0$ [curve 1 in Fig. 1(c)] and a monotonically decaying function of speed if $v_{bm}=0$ [curve 2 in Fig. 1(c)]. Eq. (3) is just a convenient and transparent way to introduce such a function.

The total EVDF of the plasma-beam system is the sum of the plasma EVDF and the beam EVDF, i.e.,

$$f(v_x,x) = f_p(v_x,x) + f_b(v_x,x), \tag{4}$$

where the beam EVDF is expressed via the VDFEE as a function of the electron total energy

$$f_b(v_x,x) = f_{b0}\left[\sqrt{v_x^2 - 2e\Phi(x)/m}\right].$$

In the case of a nonmonotonic VDFEE, the maximum of the beam EVDF is shifted relative to the plasma potential $e\Phi$ (which is also the plasma EVDF cutoff energy) by $w_{bm}=mv_{bm}^2/2$, creating the gap between the plasma and the beam on the total EVDF [see Fig. 1(d)]. Because of the gap, the total EVDF in this case does not satisfy the criterion of stability (1) for any density of emitted electrons.

In the case of a monotonically decaying VDFEE, the maximum of the beam EVDF coincides with the cutoff $v_x=v_*$ of the plasma EVDF. If

$$f_b(v_*,x) \leq f_p(v_*,x), \tag{5}$$

the total EVDF is then a monotonically decaying function of speed [see Fig. 1(e)]. Otherwise, the total EVDF increases stepwise at $v=v_*$ [see Fig. 1(f)]. Criterion (5), which in this case is equivalent to criterion (1), is satisfied if the density of emitted electrons is sufficiently low. Thus, for a collisionless plasma bounded by electron-emitting walls with a monotonically decaying VDFEE, the two-stream instability occurs only if the density of emitted electrons exceeds some threshold.

Note that criterion (5) as an equality defines a separatrix $\Gamma(\Phi_p)$ in the phase plane $\{\Phi_p,\Gamma\}$. Points below this separatrix correspond to the plasma state with a monotonically decaying total EVDF [Fig. 1(e)], while points above the separatrix describe the state where the total EVDF is nonmonotonic [Fig. 1(f)]. For a plasma with f_p given by (2) and two symmetrical counterpropagating beams with f_{b0} given by (3), the separatrix equation is

$$\Gamma = \frac{1}{2\pi^{1/2}} \frac{T_b}{T_p} \frac{n_0 v_{\text{th},p}}{a + b(T_b/T_p)^{1/2}}, \tag{6}$$

where

$$a = \exp\left(\frac{e\Phi_p}{T_p}\right)\text{erf}\left[\left(\frac{e\Phi_p}{T_p}\right)^{1/2}\right],$$

$$b = \exp\left(\frac{e\Phi_p}{T_b}\right)\text{erfc}\left[\left(\frac{e\Phi_p}{T_b}\right)^{1/2}\right],$$

$n_0=n_p+2n_b$ is the quasineutral plasma density at $x=L/2$, and $n_b=n_{b0}b$ is the electron beam density at $x=L/2$.

III. PIC SIMULATIONS WITH IMMOBILE IONS

In order to test the conclusions of the simplified analysis above, a one-dimensional collisionless plasma slab of length L with electron-emitting boundaries at $x=0$ and $x=L$ is simulated making use of a 1d3v PIC code. The PIC code is based on the direct implicit algorithm,[20,21] the code is described in detail elsewhere.[22,23] Simulations start with a uniform quasineutral plasma of density n_0 with Maxwellian EVDF of temperature T_p and immobile ions. Both boundaries are electrically grounded. At the initial stage of simulations, the boundaries absorb electrons. Due to thermal motion, the electrons from the high-energy tail of the Maxwellian EVDF leave the plasma, charging it positively relative to the walls. The electrostatic potential acquires a Π-shaped profile, with narrow high-gradient near-wall sheath regions and a plateau $\Phi(x)=\Phi_p=\text{const}$, stretching across nearly the entire system. The emission starts after a delay time t_e much larger than the electron flight time between the walls; i.e., $t_e \gg L/(2e\Phi_p/m)^{1/2}$. This procedure suppresses transitional processes related to initial massive escaping of high-energy electrons to the walls. The VDFEE is given by Eq. (3).

The walls in the considered system have equal potentials; i.e., $\Phi(0)=\Phi(L)=0$. Every electron emitted from one (source) wall reaches the opposite (target) wall if the potential profile $\Phi(x)$ is stationary. If the two-stream instability develops, the emitted electron may lose some of its energy during the flight through the plasma. If the total energy of an electron becomes negative, i.e., $\varepsilon_x=w_x-e\Phi_p<0$, it will then be reflected by the potential barrier of the sheath and will become trapped within the plasma volume. The trapping of beam electrons induced by the two-stream instability reduces the electron beam flux collected at the target wall (referred to below as the primary penetrated beam flux). The decrease of the primary penetrated beam flux in comparison with the emitted beam flux can be a characteristic of the intensity of the two-stream instability.

It is necessary to mention that in addition to the primary penetrated beam flux, the total electron flux collected by a target wall may contain a contribution from the plasma electrons and the former beam electrons, which were previously trapped by the plasma potential and performed multiple bounces between the opposite walls. These so-called weakly trapped electrons can be heated by the waves and eventually escape to the walls.[24] The weakly trapped electrons must be excluded when calculating the primary penetrated beam flux.

We discuss two simulations with immobile ions carried out with different VDFEE. These simulations have the following common parameters: $L=2.5$ cm, $n_0=10^{11}$ cm^{-3}, $T_p=12$ eV, $T_b=3$ eV, and the emission delay time is $t_e=100$ ns. Below, the beam that is emitted at $x=0$ and propagates in the positive x direction is considered.

A. Nonmonotonic VDFEE

In simulation 1, the VDFEE is nonmonotonic, with maximum at $w_{bm}=3$ eV. Note that the emitted electron beam flux [curve 1 in Fig. 2(a)] is about two times larger than the primary penetrated electron beam flux [curve 2 in Fig. 2(a)] for the duration of electron emission. This provides evidence for the two-stream instability permanently existing in the system. The phase plane $\{x,v_x\}$ of the electron beam [Fig. 2(b)] shows the development of the instability along the system. Many beam electrons are too slow by the end of their flight through the plasma to penetrate through the potential barrier near the target wall at $x=L$ [the arrow in Fig. 2(b) marks the "height" of this barrier].

The two-stream instability develops and is sustained in this simulation because the total EVDF near the emitting wall has a permanent gap between the plasma part [solid curve in Fig. 2(c)] and the beam part [dashed curve in Fig. 2(c)] and thus does not satisfy stability criterion (1). The gap of width w_{bm}, similar to the one described above [compare Fig. 2(c) with Fig. 1(d)], forms because (i) the VDFEE is nonmonotonic and (ii) the plasma EVDF near the emitting wall has a cutoff at $w_x=e\Phi_p$. The cutoff is formed because the sheath reflects only electrons with negative total energy (i.e., $w_x<e\Phi_p$ for electrons outside of the narrow sheath regions).

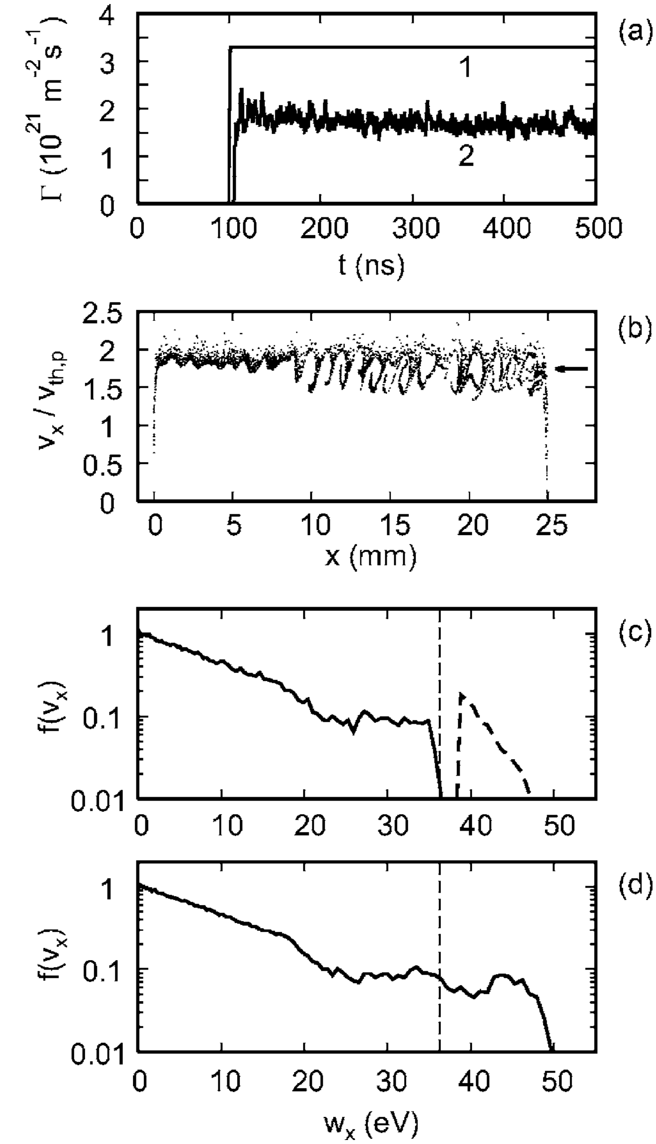

FIG. 2. For simulation with nonmonotonic VDFEE. (a) Electron flux emitted at wall $x=0$ (curve 1) and corresponding primary penetrated flux detected at wall $x=L$ versus time (curve 2). (b) Phase plane $\{x,v_x\}$ of electron beam emitted at wall $x=0$ at time 499 ns; the other wall is at $x=25$ mm. (c) EVDFs of plasma (solid curve) and beam emitted at wall $x=0$ (dashed curve) at time 499 ns averaged over the region 0.4 mm $<x<$ 0.8 mm. (d) The total EVDF at time 499 ns averaged over the region 23.5 mm $<x$ $<$ 24.5 mm. The horizontal arrow in (b) and the vertical dashed lines in (c) and (d) mark the confinement threshold energy $e\Phi_p=36.2$ eV. All EVDFs are plotted as functions of energy w_x for $v_x>0$.

Note that the plasma EVDF near the emitting wall has a plateau for 25 eV $<w_x<$ 36 eV [see the solid curve in Fig. 2(c)]. This plateau corresponds to the low-energy part (w_x $<e\Phi_p$) of the wider plateau (25eV $<w_x<$ 45eV) that forms on the total EVDF near the target wall [see Fig. 2(d)], in qualitative agreement with the predictions of the quasilinear theory[9] for the saturation stage of the two-stream instability. The electrons creating the low-energy part of the plateau are mostly trapped former beam electrons bouncing between the sheaths. Although the modification of the plasma EVDF by these electrons does not affect the beam penetration in simulation with nonmonotonic VDFEE, it becomes important for a monotonically decaying VDFEE.

B. Monotonically decaying VDFEE

In the low emission flux case, such that the total EVDF is a monotonic function of electron energy w_x, the two-stream instability does not occur and the emitted electrons freely penetrate through the plasma in the absence of collisions. Otherwise, one expects the two-stream instability to develop and the primary penetrated beam flux to weaken significantly.

In simulation 2, the VDFEE is monotonically decaying; i.e., $w_{bm}=0$. Immediately after the start of emission, the primary penetrated electron beam flux is only about one-half of the emitted electron beam flux [compare curves 1 and 2 in Fig. 3(a) for time 100 ns$<t<$130 ns]. The primary penetrated flux then grows with time, gradually approaching the emitted flux value, and for $t>300$ ns, the primary penetrated flux is about 91% of the emitted flux [see Fig. 3(a)]. The increase of the primary penetrated flux shows that in this simulation the two-stream instability appears at the initial stage of emission, but it then weakens significantly. Indeed, the electron beam phase plane $\{x,v_x\}$ obtained at $t=119$ ns shows strong perturbations typical for the instability [Fig. 3(b)], while the beam phase plane obtained at $t=499$ ns is practically unperturbed [Fig. 3(c)].

The two-stream instability develops moments after the beginning of emission because criterion (5) is not satisfied at this time. For the given emission flux [see curve 1 in Fig. 3(a)], the emission density n_{b0} is sufficiently large to ensure $f_b(v_*,x)>f_p(v_*,x)$, as one can see by comparing the plasma and beam EVDFs shown as solid and dashed curves in Fig. 3(d), respectively. Since these EVDFs are obtained near the emission wall soon after the emission starts, the plasma EVDF [solid curve in Fig. 3(d)] is almost unperturbed by the instability and is close to the cutoff Maxwellian EVDF. It is important that although the initial unperturbed plasma EVDF is characterized by the relatively low $f_p(v_*,x)$, with time the shape of the plasma EVDF changes and the value of $f_p(v_*,x)$ grows.

Similar to simulation 1, the two-stream instability creates a plateau on the total EVDF near the target wall. Due to the bouncing of trapped electrons between the walls, the plateau appears on the plasma EVDF near the emitting wall. Note that the plasma EVDF in Fig. 3(d) has a narrow plateau for 26 eV$<w_x<$31 eV. The slowed down beam electrons trapped by the plasma potential are slowly accumulated inside the plasma. This process gradually increases the plateau level of the plasma EVDF, and, respectively, the value of $f_p(v_*,x)$. The plateau growth is closely related to the presence of the instability and it continues until criterion (5) becomes satisfied near the emitting wall [compare the plateau level of the plasma EVDF shown by solid curve in Fig. 3(e) with the maximum of the beam EVDF shown by dashed curve in Fig. 3(e)]. The total EVDF then becomes a monotonic function of speed and the two-stream instability vanishes, allowing the practically unperturbed beam propagation shown in Fig. 3(c).

It is necessary to mention that this mechanism cannot suppress the two-stream instability if there is a gap between the plasma and the beam EVDF due to the nonmonotonic VDFEE, as in simulation 1.

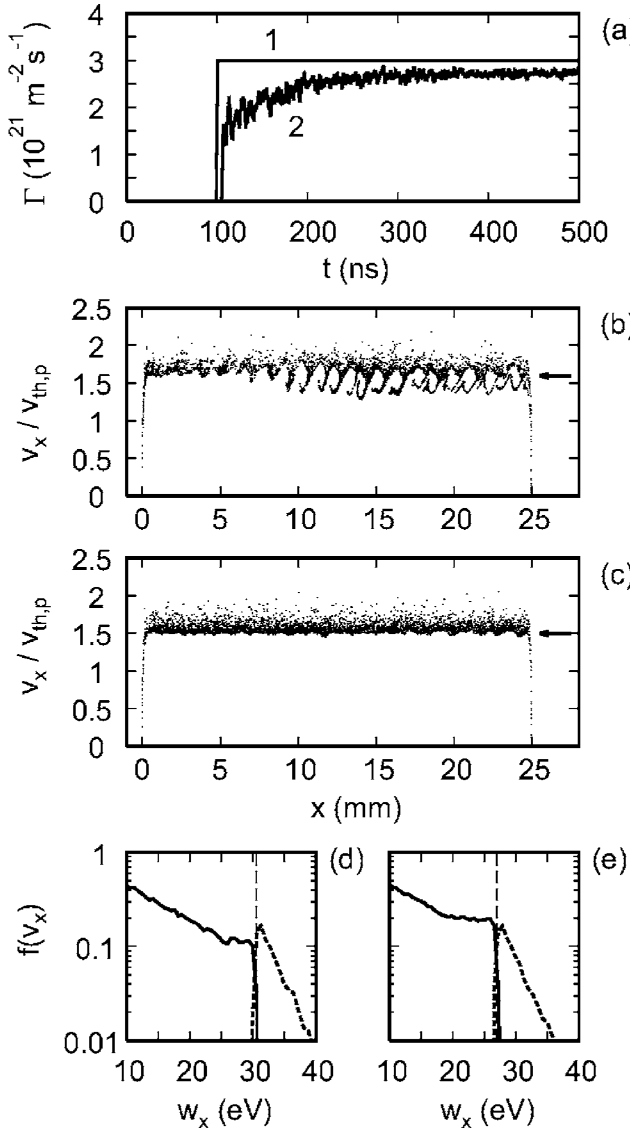

FIG. 3. For simulation with monotonically decaying VDFEE. (a) Electron flux emitted at wall $x=0$ (curve 1) and corresponding primary penetrated flux detected at wall $x=L$ (curve 2) versus time. Phase planes $\{x,v_x\}$ of electron beam emitted at wall $x=0$ at time 119 ns (b) and 499 ns (c), the other wall is at $x=25$ mm. EVDFs of plasma (solid curve) and beam emitted at wall $x=0$ (dashed curve) averaged over the region 0.5 mm$<x<$1.5 mm at time 119 ns (d) and 499 ns. (e). All EVDFs are plotted as functions of energy w_x for $v_x>0$. The horizontal arrows in (b) and (c) and the vertical dashed lines in (d) and (e) mark the confinement threshold energy, which is $e\Phi_p=31$ eV for (b) and (d) and $e\Phi_p=27$ eV for (c) and (e).

IV. TWO-STREAM INSTABILITY IN HALL THRUSTER PIC SIMULATIONS

It is instructive to verify the simulation results for the case with immobile ions described in Sec. III with those of a real physical system. Below we present some results of PIC simulations of a plane geometry Hall thruster model.[22,25] The PIC code used to do this is the same as above, but with more features enabled.

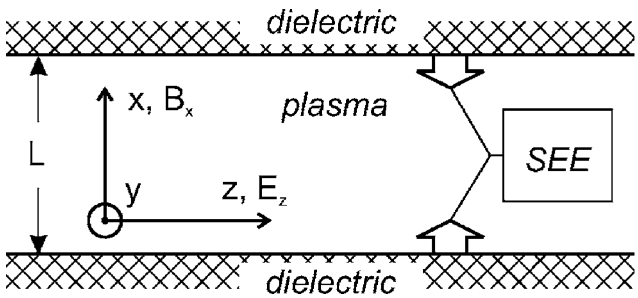

FIG. 4. Schematic diagram of the Hall thruster model. The two dielectric walls represent the coaxial ceramic channel of a Hall thruster.

The plasma in Hall thruster simulations is bounded by secondary electron-emitting dielectric walls and immersed in an external constant electric field E_z and magnetic field B_x (see Fig. 4). Both electrons and ions are treated as particles. The electron-to-ion mass ratio is that of xenon. Simulations resolve the x coordinate and the three velocity components v_x, v_y, and v_z for each particle. The electron motion is determined by the E_x, E_z, and B_x fields, while the ion motion is due to the E_x field only. The electrons perform elastic, excitation, and ionization collisions with neutral atoms with realistic frequencies for xenon.[26] Additional "turbulent" collisions that scatter electrons in the plane parallel to the walls are introduced to account for the anomalous electron mobility in Hall thrusters.[27] The SEE model[28] approximates the properties of boron nitride ceramics.[29] The one-dimensional emission EVDF is a monotonically decaying function of speed, which can be approximated by a half-Maxwellian EVDF (3) with $v_{bm}=0$ and some effective temperature T_b.

In Hall thrusters, the important parameter is the coefficient of secondary electron beam penetration defined as

$$\alpha = \frac{\Gamma_{1b}}{\Gamma_2},$$

where Γ_2 is the secondary electron flux emitted from one wall and Γ_{1b} is the flux of these electrons registered at the opposite wall (i.e., the primary penetrated beam flux). The penetration coefficient characterizes the thermalization of secondary electrons within the plasma volume and the effect of plasma cooling due to the SEE.[24,30] Due to the chosen geometry, the magnetic field B_x and the external electric field E_z cannot affect electron propagation normal to the walls. The frequency of collisions is low, so that $\lambda \gg L$. The main mechanism that decreases the energy of emitted (secondary) electrons and the primary penetrated flux of secondary electron beam is the particle-wave interaction during the two-stream instability.

In Table I, the initial parameters and results of two Hall thruster simulations are presented. Here, n_a is the neutral atom density, ν_t is the frequency of "turbulent" collisions, and T_p is the effective plasma electron temperature (in the direction normal to the walls). The values of Φ_p, T_p, T_b, n_0, Γ_2, and Γ_{1b} are obtained at the well-established stationary plasma state.

TABLE I. Initial parameters and results of Hall thruster PIC simulations.

Simulation number	3	4
L, [cm]	2.5	3.5
E_z, [V/cm]	52	200
B_x, [G]	91	100
n_a, [10^{12} cm^{-3}]	2	1
ν_t, [10^6 s^{-1}]	7.81	0.7
Φ_p, [V]	23.5	21.2
T_p, [eV]	10	12.3
T_b, [eV]	5.6	3
n_0, [10^{11} cm^{-3}]	2.31	2.25
$\Gamma_2(x=0)$, [10^{20} m^{-2} s^{-1}]	7	95.5
$\Gamma_{1b}(x=L)$, [10^{20} m^{-2} s^{-1}]	6.2	84.7
α	0.89	0.89

A. Case with low emission current

Simulation 3 with low E_z corresponds to the low-voltage regime of a Hall thruster, when SEE is weak and the secondary electron flux emitted from the walls is low.[6] In the phase plane $\{\Phi_p,\Gamma\}$, the point describing the plasma in simulation 3 is below the corresponding separatrix [compare the cross and the curve in Fig. 5(a)]. Therefore, criterion (5) is satisfied and the total EVDF should be similar to the one shown in Fig. 1(e) provided the plasma and beam EVDFs can be approximated by (2) and (3). Indeed, the plasma EVDF [solid curve in Fig. 6(b)] is strongly depleted for $w_x > e\Phi_p$, the beam EVDF [dotted curve in Fig. 6(b)] has a maximum and a cutoff at $w_x = e\Phi_p$. The total EVDF [solid curve in Fig. 6(a)] is a decaying function of speed. As a result, the instability does not develop and the beam penetration coefficient is close to unity (see Table I). Note that the total EVDF well agrees with its approximation by Eqs. (2)–(4) [dashed curve in Fig. 6(a)].

B. Case with high emission current

Simulation 4 has high E_z corresponding to the medium-voltage regime of Hall thrusters.[6] Here the SEE is much stronger and the emitted current is much more intense than in the case of low E_z. In the phase plane $\{\Phi_p,\Gamma\}$ shown in Fig. 5(b), the point (cross) describing the plasma state in simulation 4 is above the separatrix (solid curve). The corresponding approximate EVDF [dashed curve in Fig. 7(a)] given by Eqs. (2)–(4) has a beam spike. However, the actual total EVDF [solid curve in Fig. 7(a)] is a decreasing function of speed, and the beam penetration coefficient is close to unity (see Table I), which shows that the instability is absent. The mechanism that suppresses the two-stream instability here is the same as in simulation 2. Electrons with energy barely below the confinement threshold slowly accumulate to form

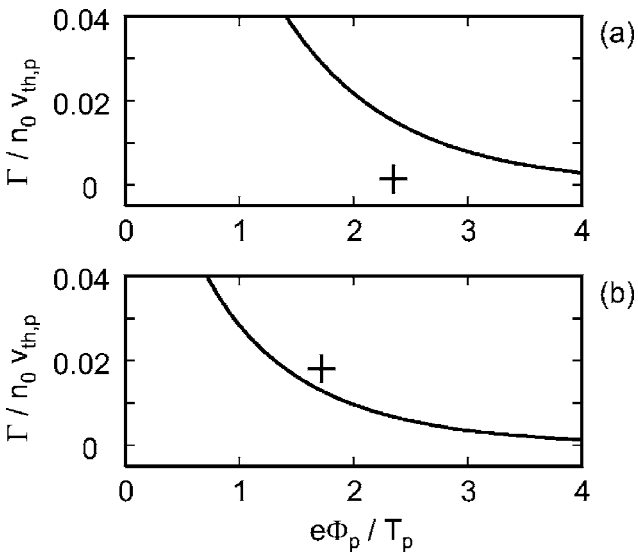

FIG. 5. Phase plane "plasma potential - emitted electron flux." (a) The cross indicates the plasma state in simulation 3, the separatrix curve is calculated by Eq. (6) with T_p/T_b=10/5.6. (b) The cross indicates the plasma state in simulation 4, the separatrix curve is calculated by Eq. (6) with T_p/T_b =12.3/3.

a small plateau on the plasma EVDF [see the solid curve in Fig. 7(b) for 15 eV$<w_x<$21 eV], increasing the value of $f_p(v_*,x)$. The electron beam [dotted curve in Fig. 7(b)] and the plasma electrons then form a monotonically decaying total EVDF stable with respect to the two-stream instability.

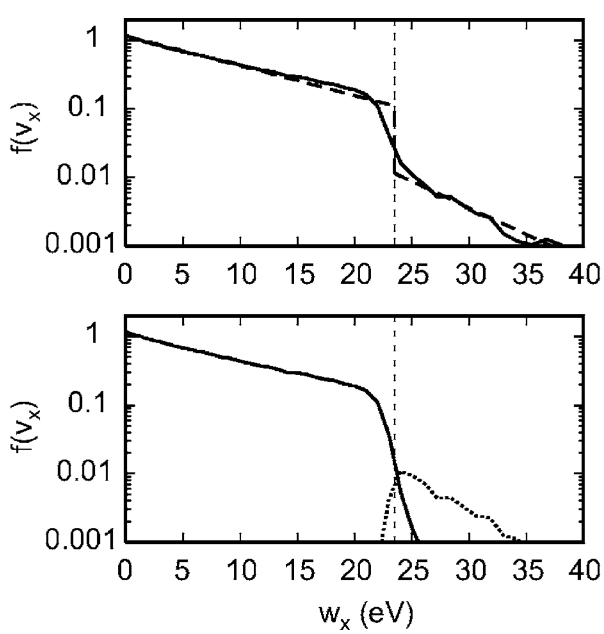

FIG. 6. EVDF over velocity normal to the walls in simulation 3 obtained in the center region 10 mm$<x<$15 mm and plotted as a function of energy $w_x=mv_x^2/2$ for $v_x>0$. (a) The solid curve is the total EVDF, the dashed curve is the approximation of the total EVDF by Eqs. (2)–(4). (b) The actual plasma EVDF (solid curve) and the actual SEE beam EVDF (dotted curve). The vertical dashed lines mark the confinement threshold energy $e\Phi_p$.

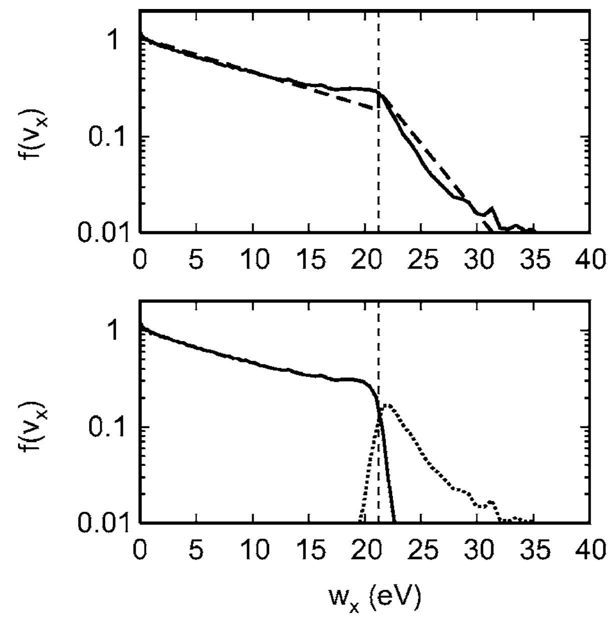

FIG. 7. EVDF over velocity normal to the walls in simulation 4 obtained in the center region 10 mm$<x<$15 mm and plotted as a function of energy $w_x=mv_x^2/2$ for $v_x>0$. (a) The solid curve is the total EVDF, the dashed curve is the approximation of the total EVDF by Eqs. (2)–(4). (b) The actual plasma EVDF (solid curve) and the actual SEE beam EVDF (dotted curve). The vertical dashed lines mark the confinement threshold energy $e\Phi_p$. Some numerical noise in the SEE beam EVDF for energies of 30–35 eV is related to the finite number of macroparticles.

V. CONCLUSIONS

In low-pressure discharges, electron emission from the walls can result in the formation of intense electron fluxes in the plasma. Examples of such emission are secondary electron emission, thermionic emission from heated metal surfaces (e.g, emissive probes), and field emission (e.g, emission from dust particles). The emitted electrons are accelerated into the plasma by the voltage drop across the sheath. The presence of such electron streams in the plasma can lead to the two-stream instability if the total electron velocity distribution function (EVDF) of the electron stream and plasma has a region with positive derivative with respect to the electron speed. If the plasma electrons are described by a Maxwellian EVDF, the combination of plasma and emitted electrons results in a nonmonotonic total EVDF leading to the two-stream instability. However, in low-pressure discharges, the EVDF is not Maxwellian, it is depleted at energies above the plasma potential relative to the wall. Therefore, the development of the two-stream instability in low-pressure discharges is different compared to Maxwellian plasmas. We performed systematic studies of the two-stream instability and found that the pattern of its development depends crucially on the shape of the velocity distribution function of electron emission (VDFEE).

One type of VDFEE considered in the present paper is a monotonically decaying function of electron energy, which starts from a positive value at zero emitted energy. The total EVDF consisting of the plasma EVDF and the VDFEE accelerated by the plasma potential is a monotonically decaying function of speed if the emission current is below some threshold. In this case, the two-stream instability does not occur. If the emission current is above this threshold so that the total EVDF is a nonmonotonic function of speed, then the two-stream instability does occur but quickly vanishes. This happens because the two-stream instability forms a plateau on the velocity distribution function of electrons confined by the plasma potential (i.e., the plasma EVDF), then the total EVDF becomes a monotonic function of speed and the beam propagates through the plasma without perturbations.

Alternatively, the VDFEE may be equal to zero at zero energy of emitted electrons and grow as a function of energy for a few electron volts. Such a nonmonotonic VDFEE is a feature of secondary electron emission from metals.[31] At low pressures, the total EVDF of the plasma-beam system near the emitting wall has a gap of a few electron volts at the energy corresponding to the wall potential. This gap is responsible for the development of the two-stream instability, which is confirmed by simulations with a nonmonotonic VDFEE. In these simulations, the two-stream instability reaches the nonlinear saturation stage and exists for as long as the emission lasts. As a result, the plasma electrons accelerate while the emitted electrons decelerate, which leads to the partial trapping of emitted electrons in the plasma. In our simulations with immobile ions and constant emission current, about 50% of emitted electrons become trapped in the plasma during their first flight between the walls. However, the two-stream turbulence accelerates these electrons back to an energy above the plasma potential so that they leave the plasma after several bounces between the walls. In fact, during a steady state, the sum of wall fluxes of emitted electrons that reach the wall after multiple bounces and those that cross the plasma directly is close to the emitted electron flux.[24] For some applications (e.g, Hall thrusters) it is therefore expedient to assume that the two-stream instability does not affect the beam propagation and that the effective penetration coefficient is close to unity.[24]

The plasmas considered in the present paper are confined by a symmetrical potential well between floating or electrically connected walls, as in Hall thrusters or hollow cathode discharges. However, even in these plasma devices, the potential profile between the walls can be nonsymmetric due to geometrical effects or applied voltage. Nevertheless, our conclusions on the effects of the VDFEE and the non-Maxwellian plasma EVDF on the two-stream instability can be generalized for plasmas with nonsymmetric potential profiles.

It is necessary to point out that the effects considered here are essentially one-dimensional and may be modified in cases in which the three-dimensional effects, such as the finite beam width, geometrical expansion in cylindrical or spherical systems, or nonuniform magnetic field effects, become important (see, e.g., Ref. 32). Electron motion along the magnetic field line is affected not only by the electrostatic force, but also by drifts in nonuniform magnetic field.[33] In addition to the electrostatic instability, where the wave number vector is parallel to the external magnetic field, two- or three-dimensional systems permit electromagnetic instabilities, where the wave number vector is nonparallel to the magnetic field.[12] To investigate these effects three-dimensional kinetic simulation is necessary.

ACKNOWLEDGMENTS

The authors thank to Artem Smirnov and Edward Startsev for helpful discussions. Simulations were carried out using the Westgrid facilities in the University of Calgary. This research was partially supported by the Air Force Office of Scientific Research and the U.S. Department of Energy Office of Fusion Energy Sciences.

[1] M. A. Lieberman and A. J. Lichtenberg, *Principles of Plasma Discharges and Materials Processing* (Wiley, New York, 2005), ISBN 0471720011.
[2] R. N. Franklin and W. E. Han, Plasma Phys. Controlled Fusion **30**, 771 (1988).
[3] N. Jelić, M. Čerček, M. Stanojević, and T. Gyergyek, J. Phys. D **27**, 2487 (1994).
[4] A. I. Akhiezer and Y. B. Fainberg, Dokl. Akad. Nauk SSSR **69**, 555 (1949), in Russian.
[5] D. Bohm and E. P. Gross, Phys. Rev. **75**, 1864 (1949).
[6] Y. Raitses, D. Staack, A. Smirnov, and N. J. Fisch, Phys. Plasmas **12**, 073507 (2005).
[7] S. I. Krasheninnikov and T. K. Soboleva, Phys. Plasmas **13**, 094502 (2006).
[8] K. V. Roberts and H. L. Berk, Phys. Rev. Lett. **19**, 297 (1967).
[9] Y. B. Fainberg, V. D. Shapiro, and V. I. Shevchenko, Sov. Phys. JETP **30**, 528 (1970).
[10] T. M. O'Neil, J. H. Winfrey, and J. H. Malmberg, Phys. Fluids **14**, 1204 (1971).
[11] N. G. Matsiborko, I. N. Onishchenko, V. D. Shapiro, and V. I. Shevchenko, Plasma Phys. **14**, 591 (1972).
[12] A. B. Mikhailovskii, *Theory of Plasma Instabilities* (Consultants Bureau, New York, 1974), Vol. 1, ISBN 0-306-17181-3.
[13] C. K. Birdsall and A. B. Langdon, *Plasma Physics via Computer Simulations* (IOP Publishing, Bristol, 1991), ISBN 0-7503-0117-1.
[14] T. Umeda, Y. Omura, H. Matsumoto, and H. Usui, J. Geophys. Res. **107**, 1449 (2002).
[15] G. D. Hobbs and J. A. Wesson, Plasma Phys. **9**, 85 (1967).
[16] L. D. Tsendin, Sov. Phys. JETP **39**, 805 (1974).
[17] I. Kaganovich, M. Misina, S. V. Berezhnoi, and R. Gijbels, Phys. Rev. E **61**, 1875 (2000).
[18] J. Schou, Phys. Rev. B **22**, 2141 (1980).
[19] P. H. Stoltz, J. P. Verboncoeur, R. H. Cohen, A. W. Molvik, J.-L. Vay, and S. A. Veitzer, Phys. Plasmas **13**, 056702 (2006).
[20] A. B. Langdon, B. I. Cohen, and A. Friedman, J. Comput. Phys. **51**, 107 (1983).
[21] M. R. Gibbons and D. W. Hewett, J. Comput. Phys. **120**, 231 (1995).
[22] D. Sydorenko, A. Smolyakov, I. Kaganovich, and Y. Raitses, Phys. Plasmas **13**, 014501 (2006).
[23] D. Sydorenko, A. Smolyakov, I. Kaganovich, and Y. Raitses, *Proceedings of the 29th International Electric Propulsion Conference, Princeton, NJ, October–November 2005* (Electric Rocket Propulsion Society, Cleveland, OH, 2005), IEPC Paper No. 2005-078.
[24] I. D. Kaganovich, Y. Raitses, D. Sydorenko, and A. Smolyakov, "Kinetic effects in a Hall thruster discharge" Phys. Plasmas (to be published).
[25] D. Sydorenko, A. Smolyakov, I. Kaganovich, and Y. Raitses, IEEE Trans. Plasma Sci. **34**, 815 (2006b).
[26] V. Vahedi and M. Surendra, Comput. Phys. Commun. **87**, 179 (1995).
[27] A. Smirnov, Y. Raitses, and N. Fisch, Phys. Plasmas **11**, 4922 (2004).
[28] V. P. Gopinath, J. P. Verboncoeur, and C. K. Birdsall, Phys. Plasmas **5**, 1535 (1998).
[29] A. Dunaevsky, Y. Raitses, and N. J. Fisch, Phys. Plasmas **10**, 2574 (2003).
[30] E. Ahedo and F. I. Parra, Phys. Plasmas **12**, 073503 (2005).
[31] M. A. Furman and M. T. F. Pivi, Technical Report SLAC-PUB-9912; LBNL-52807, 2003.
[32] E. A. Startsev and R. C. Davidson, Phys. Plasmas **13**, 062108 (2006).
[33] V. Latocha, L. Garrigues, P. Degond, and J.-P. Boeuf, Plasma Sources Sci. Technol. **11**, 104 (2002).